Journal of Alloys and Compounds 785 (2019) 871–874

Contents lists available at ScienceDirect

Journal of Alloys and Compounds

journal homepage: http://www.elsevier.com/locate/jalcom

Single crystal growth of $PtSe_2$ via CuSe flux method and its large magneto-resistance

Xiangde Zhu [a, *], Fangjun Lu [a, b]

[a] Anhui Province Key Laboratory of Condensed Matter Physics at Extreme Conditions, High Magnetic Field Laboratory, Chinese Academy of Sciences, Hefei, 230031, Anhui, People's Republic of China
[b] Department of Physics, University of Science and Technology of China, Hefei, 230026, People's Republic of China

ARTICLE INFO

Article history:
Received 16 October 2018
Received in revised form
28 December 2018
Accepted 14 January 2019
Available online 23 January 2019

Keywords:
Dirac fermions
Single crystal growth
Flux method

ABSTRACT

The type-II Dirac and Weyl fermions emerge at the topologically protected touching points of electron and hole pockets, which form highly tilted Dirac cones along certain momentum directions. Recently, the transition-metal dichalcogenide $PtSe_2$ with space group $P_{\bar{3}m1}$ was predicted as a type-II Dirac semi-metal. Though millimeter size of $PtSe_2$ single crystal grown via chemical vapor transport method has been reported, lack of large high quality single crystal hinders the further experimental research on this type-II Dirac fermions system. Here we report a successful CuSe flux method to grow $PtSe_2$ single crystal with large size of 5 mm × 5 mm × 3 mm. Transport properties of grown $PtSe_2$ single crystal are characterized.

1. Introduction

Layered transition metal dichalcogenides (TMDC) TX_2 (T = transition metal, X = S, Se, or Te) have been studied on their multiple crystal structures, charge density wave (CDW) transitions and superconductivity for decades [1–3]. The structures of layered TMDC can be regarded as the stacking of weak van-de-Waals type covalent coupled X-T-X sandwiches layers. Due to the weak van-de-Waals type coupling between layers, TMDC can be easily cleaved to a few layers or even single layer [1]. Different X-T-X coordinations and stacking sequences lead to variety crystal structures, such as 1T, 2H, 3R, 6R (number represents how many X-T-X layers in one unit cell, and capital letter represents the abbreviation of crystal systems, trigonal, hexagonal and orthorhombic, respectively) [1]. With the variation of temperature or applied pressure, some layered TMDC such as TaS_2, $IrTe_2$ endures phase transitions between different crystal structures [1,4]. During the past several years, due to the similarity to Graphene, layered TMDC such as MoS_2 and 1T-TaS_2 have attracted renewed broad interests and extensive research efforts. Pressure induced superconductivity, ion-liquid tuning induced superconductivity and thickness dependent physical properties have been discovered in MoS_2 and 1T-TaS_2 [5–10].

So far, searching for new Dirac and Weyl semi-metals has became an extensive research area, since these materials can realize the famous Dirac and Weyl fermions that come from the high energy physics basic concepts. For example, Cd_3As_2 [11] and Na_3Bi [12] were predicted and then confirmed to be type-I Dirac semi-metals, showing extreme large magneto-resistance (MR) at low temperature. TaAs, a crystal with loss of translational symmetry, was reported to be a Weyl semi-metal [13]. WTe_2, a TMDC, was reported to be a type-II Weyl semimetal featuring a large non-saturating MR [14]. Recently, 1T structure (space group $P_{\bar{3}m1}$) type $PtSe_2$ were reported as a new type-II Dirac semi-metals [15,16]. As shown in Fig. 1(a), the Pt atom is octahedrally coordinated by sixfold Te/Se atoms, with the Pt-Se distance of 2.499 Å. Viewed from the direction of *c*-axis (Fig. 1(b)), the top Se atoms have honeycomb structure. Theoretical band calculation indicates that a branch of Se 4p band crosses the Fermi level at Γ point, and that one type-II Dirac point locates at momentum space (0,0,~0.39) and ~ 1.3 eV below the Fermi level [17,18]. Different from standard type-I Dirac points with point-like Fermi surfaces, the type-II Dirac point in $PtSe_2$ appears at the contact of electron and hole pockets with strongly tilted Dirac cones. Therefore, angle-dependent chiral anomaly and topological Lifshitz transitions that are distinct from the type-I Weyl fermions known before are expected [15,16].

$PtSe_2$ film or nano-sheets has been synthesised via chemical vapor deposition method by different groups [19,20]. $PtSe_2$ single crystal with micro-meter size can be obtained via direct high

* Corresponding author.
E-mail address: xdzhu@hmfl.ac.cn (X. Zhu).

https://doi.org/10.1016/j.jallcom.2019.01.190
0925-8388/

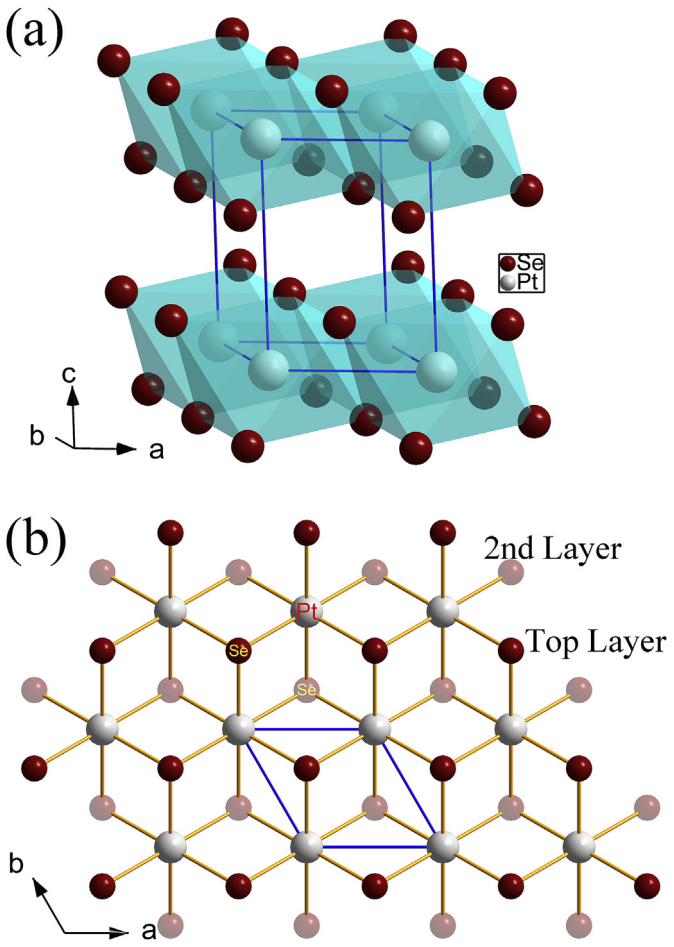

Fig. 1. (**a**) Crystal structure of $PtSe_2$. (**b**) Crystal structure of $PtSe_2$ viewed from **c**-axis.

pressure synthesised [21]. In addition, mm size $PtSe_2$ single crystal has been successfully grown via chemical vapor transport using Bromine as the transport agent [17]. However, the lack of large single crystal hinders the further confirmation of type-II Dirac semi-metal and other physical measurements. In this work, we report the successful single crystal growth of $PtSe_2$ via CuSe flux method and its physical characterization.

2. Material and methods

2.1. Synthesis

The single crystal of $PtSe_2$ was successfully grown via CuSe flux method. Our attempt of single crystal growth via Bi-Se flux method failed. In a mol ratio of 1:6:8 of Pt ribbens, Cu plates and Se pieces with high purity, were put in an alumina crucible and sealed in an evacuated quartz tube. Then the tube was put in a commercial MTI furnace. The furnace was slowly heated to 900 °C and dwelled for two days, then the furnace was decreased to 650 °C in a rate of 3 °C per hour. At this temperature, the tube was moved into a centrifuge quickly to separate the CuSe flux. As shown in Fig. 2(b), single crystals of $PtSe_2$ in shape of polyhedra can be found with the size of ~ $5 \times 5 \times 3$ mm^3. This size of the as grown $PtSe_2$ crystal is significantly larger than that of samples grown via chemical vapor transport method. The as-grown crystal can be easily cleaved along crystal face of (00*l*). The as-grown single crystal is stable in air, showing shiny silver-like faces.

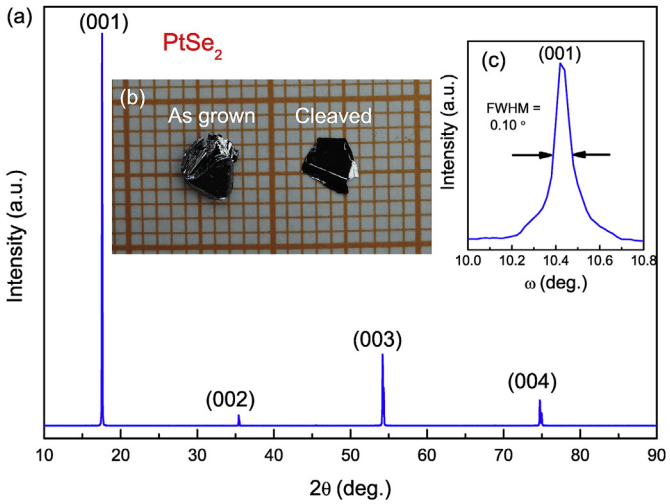

Fig. 2. (**a**) Single crystal X-ray diffraction pattern measured at room temperature for $PtSe_2$. (**b**) The photographs of as grown (left) and cleaved (right) $PtSe_2$ single crystals. (**c**) The X-ray rocking curve of (001) peak for $PtSe_2$. The full width at half maxima (FWHM) is marked as an arrow.

2.2. X-ray diffraction and elemental analysis

Several single crystals were cleaved by scotch tape for single crystal. X-ray measurement were carried on the Rigaku-TTR3 x-ray diffractometer using high intensity graphite monochromatized Cu K_α radiation. We tried to grind the single crystals into powders to measure the powder X-ray diffraction pattern, but failed to get a good pattern due to the strong preferred orientation of (00*l*) crystal face. Elemental analysis was performed by using energy-dispersive X-ray spectroscopy (EDS) on an FEI Helios Nanolab 600i. The EDS results gives a Pt:Se ratio very close to 1:2, which indicates the good stoichiometry of the as-grown sample.

2.3. Transport properties and magnetism

Electrical transport measurement was carried out on a Quantum Design Physical Property Measurement System, with the current applied along in-plane direction. Data were collected over a temperature range of 2–300 K. Temperature dependent resistivity and MR measurement were performed using a four-probe configuration. Gold wires were attached on a polished sample with the electrical contacts made of silver paint.

3. Results and discussion

Fig. 2(a) shows the X-ray diffraction pattern of $PtSe_2$ single crystal measured at room-temperature. Obviously, the diffraction peaks corresponding to (00*l*) crystal faces can be observed. Interestingly, the heights of (001), (003), and (004) peaks are significantly higher than that of (002) peak. This result roughly follows the previous result of the intensity ratio 509:2.4:27:35 for (001):(002):(003):(004) peaks [22]. Fig. 2(c) shows the X-ray rocking curve of (001) peak for $PtSe_2$. The full width at half maxima (FWHM) is about 0.1°, which indicates the high quality of the grown single crystal.

Fig. 3(a) shows the temperature dependence of in-plane resistivity (ρ_{ab}) for $PtSe_2$. Obviously, ρ_{ab} increases with increasing temperature below 300 K, indicating a typical behavior of a non-magnetic metal or semi-metal. The residual resistivity ratio (RRR) is about 6. As a non-magnetic metal, the scattering mechanism of charges is mainly acoustic phonon scattering. Bloch-Grüneisen (BG)

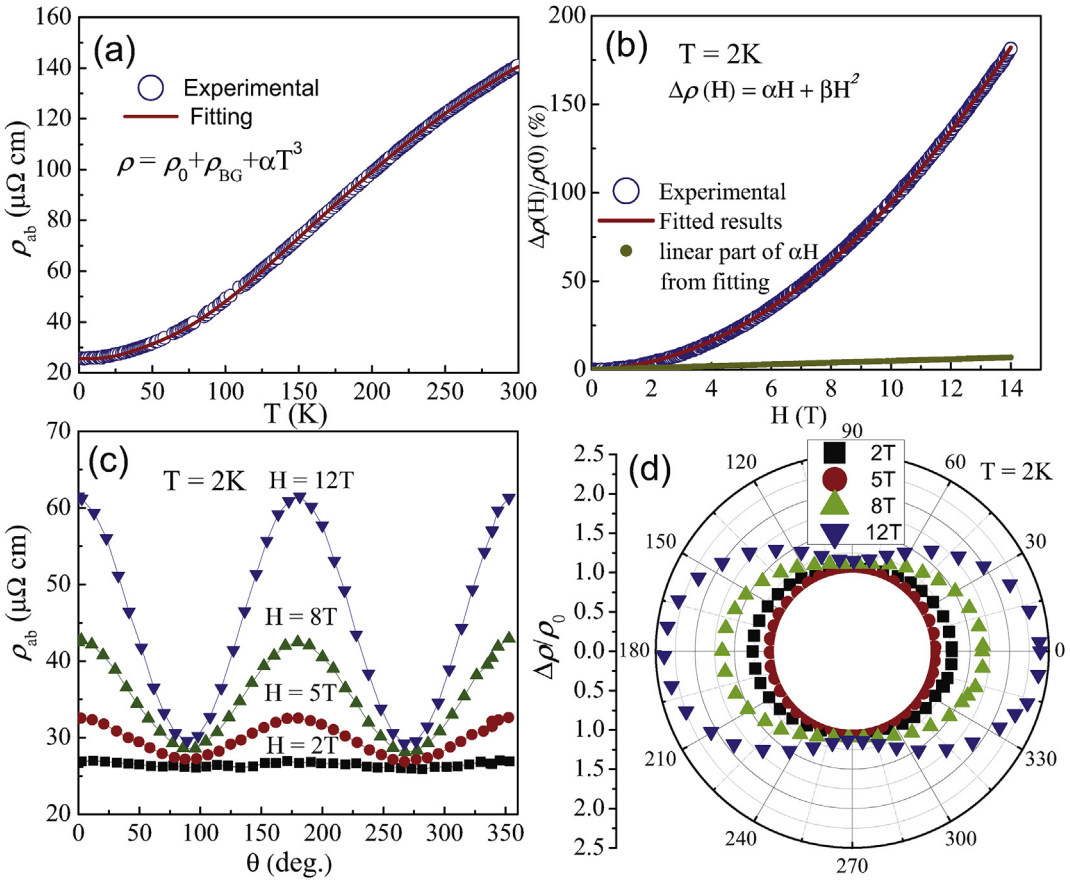

Fig. 3. (**a**) The temperature dependence of in-plane resistivity ρ_{ab} (blue open circle) and its fitting result (red line) for $PtSe_2$. (**b**) The field dependence of ρ_{ab} for $PtSe_2$ measured at T = 2 K (blue open circle). The red solid line represents the extrapolating fitting results from the data between 0 < H < 5 T. The brown small solid dot represents the linear part contribution from the fitting. (**c**) Angular dependence of ρ_{ab} for $PtSe_2$ measured at T = 2K and H = 2, 5, 8, 12 T as labeled. (**d**) Polar plot of angular dependence of ρ_{ab} for $PtSe_2$ measured at T = 2 K and H = 2, 5, 8, 12 T. (For interpretation of the references to colour in this figure legend, the reader is referred to the Web version of this article.)

formula with $n \sim 3$ or 5

$$\rho_{BG} = \rho_0 + A_{ac}\left(\frac{T}{\Theta_R}\right)^n \int_0^{\frac{\Theta_R}{T}} \frac{x^n}{(e^x - 1)(1 - e^{-x})} dx \quad (1)$$

is widely used to explain temperature dependence of ρ_{ab} for various non-magnetic materials and good metals, where ρ_0 is the residual resistivity, ρ_{BG} is contribution part from the electron-phonon scattering, A_{ac} is the coefficient of electron-phonon inter-action, Θ_R is the Debye temperature [23,24]. We failed to fit the data with the simple BG model. Because of the two-dimensional structure of $PtSe_2$, the in-plane and out-of-plane acoustic phonons should have different frequencies, which further leads to two different Debye temperatures. Therefore, we propose a modified BG formula (n = 5) with taking the contribution of s-d electron inter-band scattering into account

$$\rho(T) = \rho_0 + \rho_{BG1} + \rho_{BG2} + \alpha T^3 \quad (2)$$

where αT^3 term representing the contribution of s-d electron inter-band scattering [25]. The fitted data shown as red (drak) line in Fig. 3(a) overlaps with experimental data very well in the whole measured temperature range. The obtained A_{ac1} is 0.62 $\mu\Omega$cm K^{-1}, A_{ac2} is 0.62 $\mu\Omega$cm K^{-1}, Θ_{R1} is 135 K, Θ_{R2} is 580 K, α is 1.08×10^{-6} $\mu\Omega$cm K^{-3}.

Fig. 3(b) shows the field dependence of transverse MR for $PtSe_2$ measured at T = 2 K. The field dependence of MR can be fitted well to a relation of $\Delta\rho = \alpha H + \beta H^2$(the obtained α is 0.0049 $\mu\Omega$cm T^{-1}, β is 0.00894 $\mu\Omega$cm T^{-2}), rather than the semi-classic power law $\Delta\rho \propto H^2$ for typical metal. The deduced linear part of the field dependence of MR is plotted in Fig. 3(b) as brown solid dot, indicating that the linear term is the minor part. The linear contribution of MR is typical in $SrMnBi_2$ [26], Ag2 − δ(Te/Se) [27,28] and other topological insulators, whose electronic band structure have a linear energy spectrum in the quantum limit. As mentioned above in the introduction, band calculation results give that the Fermi level is dominated by the metal branch of Se 4p band, and that there is a Type-II dirac cone below the Fermi level. This can explain that why the MR for $PtSe_2$ have the dominate classic H^2 term and minor linear H term. In addition, the MR reaches 180% at H = 14 T, which is significantly larger than that of normal metal. This value is comparable to the 115% MR at H = 9T for $SrMnBi_2$, which is a typical two-dimensional Dirac fermions system.

Fig. 3(c) shows the angular dependence of MR for $PtSe_2$ measured at T = 2 K and H = 2, 5, 8, 12 T. The angular dependence of MR is extracted from Fig. 3(c) and polar-plotted in Fig. 3(d). Obviously, a classical two fold symmetry MR can be observed. In contrast, the MR of triply degenerate point fermions system $PtBi_2$ reaches the maximum value when the field is applied titled with $\theta = 30°$ [29].

In summary, single crystals of $PtSe_2$ were grown via flux method using CuSe as the flux. The size of the as grown crystal is as large as $5 \times 5 \times 3$ mm^3, which is significantly larger than those grown via

chemical vapor transport method. The X-ray diffraction pattern and rocking curve indicate that the single crystal is of the high quality. The temperature dependence of resistivity, MR and angular dependent MR were measured, indicating that $PtSe_2$ is not a simple metal with a relatively large MR of 180% up to 14 T at T = 2 K. Further investigations are needed to figure out that whether the angle-dependent chiral anomaly and the topological Lifshitz transitions exist in $PtSe_2$ or not.

Acknowledgements

Work at High magnetic field lab (Hefei) was supported by The National Key Research and Development Program of China(Grant No.2017YFA0403502), National Natural Science Foundation of China (Grants No.11474289) and Youth Innovation Promotion Association CAS(Grant No.2017483).

References

[1] F.J. Disalvo, J.A. Wilson, S. Mahajan, Charge-density waves and superlattices in the metallic layered transition metal dichalcogenides, Adv. Phys. 24 (2) (1975) 117–201.
[2] J.J. Yang, A. Hogan, Y. Horibe, K. Kim, B.I. Min, Y.J. Choi, Y.S. Oh, S.-W. Cheong, Charge-orbital density wave and superconductivity in the strong spin-orbit coupled $IrTe_2$:Pd, Phys. Rev. Lett. 108 (11) (2012), 116402.
[3] P.D. Johnson, J. Xue, K.E. Smith, T. Valla, A.V. Fedorov, F.J. DiSalvo, Charge-density-wave-induced modifications to the quasiparticle self-energy in 2H-TaS_2, Phys. Rev. Lett. 85 (2000) 4759–4762.
[4] Yoon Seok Oh, J.J. Yang, Y. Horibe, S.-W. Cheong, Anionic depolymerization transition in $IrTe_2$, Phys. Rev. Lett. 110 (2013), 127209.
[5] James Hone, Jie Shan, Kin Fai Mak, Changgu Lee, F. Tony, Heinz. Atomically thin MoS_2: a new direct-gap semiconductor, Phys. Rev. Lett. 105 (2010), 136805.
[6] Q.H. Wang, K. Kalantar-Zadeh, Andras Kis, Jonathan N. Coleman, Michael S. Strano, Electronics and optoelectronics of two-dimensional transition metal dichalcogenides, Nat. Nanotechnol. 7 (11) (2012) 699–712.
[7] Zhenhua Chi, Xuliang Chen, Fei Yen, Feng Peng, Yonghui Zhou, Jinlong Zhu, Yijin Zhang, Xiaodi Liu, Chuanlong Lin, Shengqi Chu, Yanchun Li, Jinggeng Zhao, Tomoko Kagayama, Yanming Ma, Zhaorong Yang, Superconductivity in pristine $2H_aMoS_2$ at ultrahigh pressure, Phys. Rev. Lett. 120 (2018), 037002.
[8] M.S. Bahramy, Y. Kohama, J.T. Ye, Y. Kasahara, Y. Nakagawa, M. Onga, M. Tokunaga, T. Nojima, Y. Yanase, Y. Saito, Y. Nakamura, Y. Iwasa, Superconductivity protected by spin-valley locking in ion-gated MoS_2, Nat. Phys. 12 (2) (2016) 144.
[9] A. Akrap, H. Berger, L. Forro, B. Sipos, A.F. Kusmartseva, E. Tutis, From mott state to superconductivity in 1T-TaS_2, Nat. Mater. 7 (12) (2008) 960–965.
[10] Xiu Fang, Lu Ya, Jun Yan, Yong-Heum Cho, Liguo Ma, Xiaohai Niu, Sejoong Kim, Young-Woo Son, Donglai Feng, Shiyan Li, Sang-Wook Cheong, Xian Hui Chen, Yijun Yu, Fangyuan Yang, Yuanbo Zhang, Gate-tunable phase transitions in thin flakes of 1T-TaS_2, Nat. Nanotechnol. 10 (3) (2015) 270–276.
[11] D. Evtushinsky, V. Zabolotnyy, B. Büchner Bernd, S. Borisenko, Q. Gibson, Robert J. Cava, Experimental realization of a three-dimensional Dirac semimetal, Phys. Rev. Lett. 113 (2014), 027603.
[12] Z.K. Liu, B. Zhou, Y. Zhang, Z.J. Wang, H.M. Weng, D. Prabhakaran, S.-K. Mo, Z.X. Shen, Z. Fang, X. Dai, Z. Hussain, Y.L. Chen, Discovery of a three-dimensional topological Dirac semimetal, Na_3Bi, Science 343 (6173) (2014) 864–867.
[13] B.Q. Lv, H.M. Weng, B.B. Fu, X.P. Wang, H. Miao, J. Ma, P. Richard, X.C. Huang, L.X. Zhao, G.F. Chen, Z. Fang, X. Dai, T. Qian, H. Ding, Experimental discovery of weyl semimetal TaAs, Phys. Rev. X 5 (2015), 031013.
[14] Steven Flynn, Jing Tao, Quinn D. Gibson, Leslie M. Schoop, Tian Liang, Neel Haldolaarachchige, Max Hirschberger, N.P. Ong Mazhar, N. Ali, Jun Xiong, R.J. Cava, Large, non-saturating magnetoresistance in WTe_2, Nature 514 (7521) (2014) 205.
[15] L. Muechler, L.S. Xie, M. Hirschberger, N.P. Ong, R. Car, R.J. Cava, Q.D. Gibson, L.M. Schoop, Three-dimensional Dirac semimetals: Design principles and predictions of new materials, Phys. Rev. B 91 (2015), 205128.
[16] Huaqing Huang, Shuyun Zhou, Wenhui Duan, Type-ii Dirac fermions in the $PtSe_2$ class of transition metal dichalcogenides, Phys. Rev. B 94 (2016), 121117.
[17] Haoxiong Zhang, Huaqing Huang, Masashi Arita, Zhe Sun, Wenhui Duan, Yang Wu, Kenan Zhang, Mingzhe Yan, Shuyun Zhou, Experimental evidence for type-ii Dirac semimetal in $PtSe_2$, Phys. Rev. B 96 (2017), 125102.
[18] Sandy Adhitia Ekahana, Nitesh Kumar, Juan Jiang, Lexian Yang, Cheng Chen, Chaoxing Liu, Binghai Yan, Claudia Felser, Gang Li, Zhongkai Liu, Yiwei Li, Yunyouyou Xia, Yulin Chen, Topological origin of the type-ii Dirac fermions in $PtSe_2$, Phys. Rev. Mater. 1 (2017), 074202.
[19] Xue Zhou, Guangqi Zhang, Hongyun Zhang, Kenan Zhang, Wei Yao, Nianpeng Lu, Shuzhen Yang, Shilong Wu, Tomoki Yoshikawa, Koji Miyamoto, Taichi Okuda, Yang Wu, Pu Yu, Wenhui Duan, Mingzhe Yan, Eryin Wang, Shuyun Zhou, High quality atomically thin ptse 2 films grown by molecular beam epitaxy, 2D Mater. 4 (4) (2017), 045015.
[20] Zegao Wang, Qiang Li, Flemming Besenbacher, and Mingdong Dong. Facile synthesis of single crystal ptse2 nanosheets for nanoscale electronics. Adv. Mater., 28(46):10224–10229.
[21] Ke Liu, Binjie Zheng, Jingjun Wu, Yuanfu Chen, Xinqiang Wang, Fei Qi, Duanwei He, Wanli Zhang, Yanrong Li, Synthesis of two-dimensional semiconductor single-crystal ptse2 under high pressure, J. Mater. Sci. 53 (2) (2018) 1256–1263.
[22] Crystal growth and characterization of several platinum sulfoselenides, Mater. Res. Bull. 11 (8) (1976) 927–932.
[23] N.F. Mott, H. Jones, The Theory of the Properties of Metals and Alloys, Oxford University Press, London, 1936, pp. 268–280.
[24] Abhishek Pandey, R.J. Goetsch, V.K. Anand, D.C. Johnston, Structural, thermal, magnetic, and electronic transport properties of the $LaNi_2(Ge_{1-x}P_x)_2$ system, Phys. Rev. B 85 (2012), 054517.
[25] N.F. Mott, The resistance and thermoelectric properties of the transition metals, Proc. Roy. Soc. Lond. A Math. Phys. Eng. Sci. 156 (888) (1936) 368–382.
[26] Hechang Lei, S.W. Tozer, Kefeng Wang, D. Graf, Petrovic, Quantum transport of two-dimensional Dirac fermions in $SrMnBi_2$, Phys. Rev. B 84 (2011), 220401.
[27] T.F. Rosenbaum, M.-L. Saboungi, J.E. Enderby, R. Xu, A. Husmann, P.B. Littlewood, Large magnetoresistance in non-magnetic silver chalcogenides, Nature(Lodon) 390 (1997) 5760.
[28] M.-L. Saboungi, M. Lee, T.F. Rosenbaum, H.S. Schnyders, Band-gap tuning and linear magnetoresistance in the silver chalcogenides, Phys. Rev. Lett. 88 (2002), 066602.
[29] Fawei Zheng-Min, Wu-Jinglei Zhang, Chuanying Xi, Ping Zhang, Yuheng Zhang, Ning Hao, Wei Ning, Wenshuai Gao, Xiangde Zhu, Mingliang Tian, A possible candidate for triply degenerate point fermions in trigonal layered PtBi2, Nat. Commun. 9 (2018) 3249.